Deferasirox Shows Inhibition Activity Against Cervical Cancer *in vitro* and *in vivo*

Nan Zhou
Hebei Normal University
Yan Cui
Hebei Normal University
Yuhuan Kuang
Hebei Normal University
Jianyuan Hou
Hebei Normal University
Yumeng Zhu
Hebei Normal University
ShuBo Chen
Xingtai People's Hospital
Xin Xu
Xingtai People's Hospital
Ke Tan
Hebei Normal University
Pengxiu Cao
Hebei Normal University
Xianglin Duan
Hebei Normal University
Fan yumei (yumei_f1@163.com)
Hebei Normal University https://orcid.org/0000-0002-1856-5136

Research article

Keywords: Deferasirox, cervical cancer, iron chelation

Posted Date: July 16th, 2020

DOI: https://doi.org/10.21203/rs.3.rs-41539/v1

Abstract

Background: Iron depletion may be a novel therapeutic strategy for cancer. As an oral iron chelator, deferasirox (DFX) is expected to become an anticancer agent. This study aimed to assess the effects of DFX on cervical cancer.

Methods: The effects of DFX on cellular iron metabolism, cell viability, cell cycle and apoptosis, and cell invasion were assessed in two cervical cancer cell lines. The effects of DFX on the expression of cell cycle regulators cyclin D1, cyclin E and proliferating cell nuclear antigen (PCNA) were examined. The expression of N-myc downstream regulated gene 1 (NDRG1) and c-myc, and the activation of the MEK/ERK signaling pathway were investigated. The effect of DFX on tumor burden was assessed using a murine xenograft model.

Results: DFX decreased the viability of HeLa and SiHa cells, induced cell cycle and apoptosis, and decreased cell invasion. The expression of NDRG1 was upregulated while that of c-myc was downregulated. The activation of the MEK/ERK signaling pathway was inhibited by DFX. DFX also significantly suppressed xenograft tumor growth with no serious side effects, decreased ferritin levels in nude mice serum, and decreased ferritin heavy chain (FTH) expression in xenograft tumor tissue.

Conclusions: The inhibitory effect of DFX on cervical cancer cells and xenograft tumor growth was related to its effective depletion of iron in tumor cells**.** These results demonstrate that DFX has potential as a therapeutic agent for cervical cancer.

Background

Cervical cancer is the fourth most common cancer in women worldwide, with 85% of cases occurring in developing countries, where cervical cancer is the leading cause of cancer death in women [1]. The 3-year to 5-year survival rate from cervical cancer (all stages), for many underdeveloped countries is < 50% [2]. Surgical resection and adjuvant radiotherapy are usually used in the treatment of early cervical cancer cases. The majority of advanced stage cervical cancer is incurable and ultimately develops recurrences and metastasis, with subsequent mortality [3]. As such, new therapeutic approaches are needed.

Iron is an essential element that facilitates cell replication, metabolism and growth [4]. Since tumor cells exhibit an iron-seeking phenotype achieved through dysregulation of iron metabolic proteins, iron chelators have been shown to inhibit the proliferation of cancer cells and/or induce the apoptosis of cancer cells from patients with leukemia, hepatocellular carcinoma, pancreatic cancer and neuroblastoma [5–8]. In clinical studies, the potential benefit of iron chelators on inhibition of tumor growth has also been investigated, and promising results have been obtained in patients with leukemia and neuroblastoma [9, 10]. Simonart et al. demonstrated that deferoxamine (DFO), a standard iron chelator, has anti-proliferative and apoptotic effects on human cervical carcinoma cells [11]. However, it fails to prevent the growth of SiHa-induced tumors in mice [12]. A possible explanation for this lack of in

vivo antitumor activity of DFO could be related to its short circulation half-life, which will limit its clinical application.

In the present study, we showed the inhibitiory activity of a new oral iron chelator, deferasirox (DFX), against cervical cancer in *vitro* and in *vivo*.

Methods

Cell culture

Human cervical cancer cell lines, HeLa and SiHa, were obtained from American Type Culture Collection (ATCC, Manassas, VA, USA) and cultured in DMEM (Gibco-BRL, Garlsbad, CA, USA) supplemented with 10% fetal bovine serum and 1% penicillin-streptomycin. Culture medium was changed every 2–3 days and the cells were sub-cultured when 80% confluent. All cells were incubated at 37°C in a humidified atmosphere containing 5% CO_2.

Reagents

The antibody for transferrin receptor 1 (TfR1) was purchased from Invitrogen (Carlsbad, CA, USA). Antibody for FTH was purchased from Abcam (Cambridge, MA, USA). Antibodies against cyclin D1, cyclin E, proliferating cell nuclear antigen (PCNA), c-myc, p-ERK, ERK, p-c-Raf, and p-MEK1/2 were obtained from Cell Signaling Technology (Danvers, MA, USA). Antibody for N-myc down-stream-regulated-gene 1 (NDRG1) was purchased from Proteintech (Wuhan, China). All secondary antibodies used for western blotting and immunohistochemistry were purchased from KPL (Gaithersburg, MD, USA). Cell counting kit-8 (CCK-8) was purchased from MCE (Princeton, NJ, USA). PE Annexin V Apoptosis Detection Kit I was purchased from BD Biosciences (San Diego, CA, USA). Propidium iodide (PI) buffer was purchased from Invitrogen (Carlsbad, CA, USA). DFX was obtained from Novartis (Basel, Switzerland). For in *vitro* studies, DFX was dissolved in dimethyl sulfoxide at a stock concentration of 100 mM. For in *vivo* studies, DFX was dissolved in a sodium chloride solution (0.9% w/v; CSPC PHARMA. Shijiazhuang, Hebei, China).

Serum parameters

Mouse serum ferritin levels were measured by the enzyme-linked immunoassay method (Mouse Ferritin ELISA kit, Kamiya Biochemical Company, Seattle, WA, USA). Other mouse serum parameters were analyzed by the Laboratory Department of Xingtai People's Hospital. White blood cells (WBC), red blood cells (RBC), hemoglobin and platelets were analyzed using multiparameter automated hematology analyzers (Sysmex xs-500i, Sysmex Corporation, Kobe, Hyogo, Japan). Serum biochemistry, including total protein, albumin, alanine transaminase, aspartate transaminase, alkaline phosphatase, and blood urea nitrogen, were measured using automatic biochemistry analyzer (Hitachi 7600 automatic biochemical analyzer, Hitachi, Ltd, Tokyo, Japan).

Immunohistochemistry (IHC)

Paraffin-embedded mouse tissue samples were cut into 4 μm sections, which were deparaffinized with dimethylbenzene and rehydrated. For antigen retrieval, the slides were pretreated with 0.01 M citrate buffer (pH 6.0), prior to being heated in a microwave oven for 15 min. Sections were treated with 3% hydrogen peroxide to inactivate endogenous peroxidase for 15 min at 25°C, and then incubated with an FTH rabbit monoclonal antibody (1:250 dilution; Abcam, Inc. Cambridge, MA, USA) overnight at 4 °C. Subsequently, the sections were incubated with an HRP-conjugated secondary antibody at room temperature for 30 min. After that, protein expression was visualized using 3.3'-diaminobenzidine hydrochloride, and these sections were stained with hematoxylin. Sections incubated with goat serum were used as a negative control. Finally, two senior pathologists who were blinded to the patients' information evaluated the staining intensity of the sections.

Cell counting kit-8 (CCK-8) assay

Cells were seeded in a 96-well plate (5,000 cells/well) and incubated at 37 °C for 24 h. Increasing concentrations (0–200 μM) of DFX were then added to each well, and the cells were incubated for 24, 48, or 72 h. At the end of the culture period, cell viability was determined by the CCK-8 assay according to the manufacturer's instructions. The absorbance was measured at 450nm with a hybrid reader (Synergy H4, BioTek Instruments, VT, USA). Each sample had five duplicate wells and was independently performed in triplicate.

Cell cycle analysis

HeLa and SiHa cells were plated in 6-well plates at 2×10^6/well for 24h. After incubation with DFX (0–200 μM) for 24h, the cells were incubated in 70% cold alcohol overnight at 4 °C. Subsequently, a total of 1×10^6 cells were resuspended in 500 μL of PBS to which 100 μL RNAse A (Keygen Biotech, Nanjing, China) and 500 μL PI buffer were added. After incubation in darkness for 30 min at 37 °C, cell cycle phase distribution was assayed using a Beckman Coulter FC 500 type flow cytometer (Beckman Coulter, Miami, FL, USA) and the data were analyzed by multicycle AV for Windows software (Beckman Coulter, Miami, FL, USA). The results are indicated as mean values from three independent determinations.

Apoptosis analysis

An Annexin Ⅴ-FITC/PI apoptosis kit (Sigma-Aldrich, St. Louis, MO, USA) was used to detect apoptosis in HeLa and SiHa cells. Cells were cultured as described above and washed with PBS, and then resuspended in 500 μL binding buffer containing 5 μL Annexin Ⅴ-FITC and 5 μL PI for 30 min in dark condition at room temperature. Apoptotic cells were detected using a Beckman Coulter FC 500 flow cytometer and analyzed using the Expo32-ADC software (Beckman Coulter, Miami, FL, USA). All assays were performed in triplicates.

Cell invasion assay

The invasion ability of cells was measured using a Transwell chamber. For the cell invasion assay, Matrigel (Corning, NY, USA) was place between the upper and lower compartments. Aliquots of cells (1×10^5 in 200 μL) were seeded in the upper compartment of the 24-well Transwell chamber and incubated in serum-free medium with 50 μM DFX for 24 h. The lower compartment's culture medium contained 50 μM DFX and 10% FBS. After 24 h, cells remaining on the upper surface of the membrane were removed, and the cells that migrated through the membrane were fixed and stained with crystal violet. Stained cells were visualized and counted under a light microscope. The assay was performed in triplicate and repeated three times.

qRT-PCR analysis

Cells were collected, and total RNA was extracted from cells using Trizol reagent (Invitrogen Life Technologies, Carlsbad, CA, USA) and the cDNA was synthesized by reverse transcription according to the manufacturer's protocol using an RT-kit (BioTeke Corporation, Beijing, China). The qPCR analyses were performed with SYBR Green using BIO-RAD CFX Connect Real-Time System (Hercules, CA, USA). The PCR conditions were as follows: 10 min at 95°C, followed by 40 cycles of 15 s at 95°C and 60 s at 60°C. The relative levels of mRNA expression were analyzed by the $2^{-\Delta\Delta Ct}$ method with based on the cycle threshold (Ct) values using β-Actin as an internal control. PCR was performed using the following primers: NDRG1 forward 5'-TCACCCAGCACTTTGCCGTC-3' and reverse 5'-GCCACAGTCCGCCATCTT-3'; c-myc forward 5'-CTCCAGCTTGTACCTG-3' and reverse 5'-GTTGTGCTGATGTGTGGAG-3'; β-actin forward 5'-GTCGTCGACAACGGCTC-3' and reverse 5'-GCACAGTGTGGGTGA-3'. The experiments were repeated a minimum of three times.

Western blot

HeLa and SiHa cells were lysed in RIPA buffer with protease inhibitors (1 μg/mL aprotinin, 1 μg/mL leupeptin, and 1 mM phenylmethylsulfonyl fluoride) or phosphatase inhibitors (Phosphatase Inhibitor Cocktail, Roche). Protein concentration was detected using BCA protein assay kit (Applygen, Beijing, China). Twenty micrograms of protein was separated on a 12% SDS-PAGE gel and transferred to PVDF membranes (Roche Life Science, Basel, Switzerland). After blocking the membrane with 5% non-fat milk for 2 h at room temperature, the targeted proteins were incubated overnight at 4 °C with the following specific primary antibodies: FTH, TfR1, ferroportin 1 (FPN1), cyclin D1, cyclin E, p-ERK, ERK, p-c-Raf (Ser338), p-MEK1/2, PCNA, NDRG1, c-myc, and β-actin. Thereafter, the membranes were washed and exposed to peroxidase-conjugated secondary antibodies (anti-rabbit or anti-mouse). Finally, the membranes were detected with an enhanced chemiluminescence detection kit (Wanleibio, Shenyang, China). The total density of the protein bands was detected using the LAS4000 System (FujiFilm).

Animal model and DFX administration

Female BALB/c nude mice (18–19 g; 5–6 weeks old) were obtained from Beijing HFK Bioscience CO., LTD (Beijing, China) (SCXK: 2014-0004). All animals were bred and maintained at the Experimental Animal Center, Hebei Normal University (Shijiazhuang, China). The animal experimental protocol was established

according to the ARRIVE guidelines and was approved by the Laboratory Animal Ethical and Welfare Committee（AEWC）of Hebei Normal University. Mice were maintained under sterile airflow conditions and housed under a 12 h light-dark cycle, routinely fed basal rodent chow, and watered ad libitum throughout the experiments. In order to induce subcutaneous (s.c.) tumor formation, HeLa cells (1×10^7) were suspended in 0.5 mL PBS and injected subcutaneously into the right thigh of each mouse. After engraftment, tumor size was measured every 2 days, and tumor volume (TV) was calculated as follows: TV (mm^3) = ($width^2 \times length$) /2.

Approximately 2 weeks after the injection (average tumor volume, 150 mm^3), DFX treatment began. The mice were randomly separated into three groups (n = 8 per group) as follows: the control group, low-dose (100 mg/kg) DFX-treated, and high-dose (200 mg/kg) DFX-treated groups. The control group (n = 8) was treated with the vehicle alone (saline solution). The drug was administered by oral gavage every other day for 3 weeks. The health of the mice was assessed by measuring weight and monitoring behavior. The tumor volume was measured and calculated three times per week. The tumor inhibition rate (%) was calculated based on the formula (TV of control group – TV of treatment group)/TV of control group × 100%. The experiments were terminated if the tumor volume of the control group reached 1500 mm^3, or if the tumor volume of the DFX-treated group coexisted with their host at a stable size. At the end of the experiment, the mice were anesthetized and exsanguinated by direct cardiac puncture, and blood was retained for full blood count and biochemical analysis. Tumors were excised and weighed to assess tumor burden and divided into several samples for IHC.

Data and Statistical Analysis

Values are expressed as mean ± SD. The data were analyzed using SPSS statistical software (version 20.0 for Windows SPSS, Inc., Chicago, IL, USA). The mean difference was determined by Student's *t*-test, one-way ANOVA, and Chi-square tests. Values of $p < 0.05$ were considered statistically significant.

Results

Effect of DFX on the expression of iron metabolism proteins in cervical cancer cell lines

To assess the ability of DFX to mobilize cellular iron levels, HeLa and SiHa cells were incubated with the indicated concentrations of DFX (0–200 μM) for 48 h. The protein levels of TfR1 (the receptor of iron carrier transferrin), FTH (one of the subunits of the cellular iron storage protein ferritin), and FPN1 (the cellular iron exporter) were measured using western blot. As shown in Figure 1, DFX treatment increased the protein level of TfR1 in a dose-dependent manner but decreased the protein levels of FTH and FPN1. This result indicates that DFX reduced the iron levels in HeLa and SiHa cells.

DFX inhibits the viability of cervical cancer cell lines

To examine the anti-proliferative activity of DFX against cervical cancer in *vitro*, HeLa and SiHa cells were incubated with indicated concentrations of DFX (0–200 μM) for 0, 24, 48, and 72 h. Cell viability was

determined by the CCK-8 assay. As shown in Figure 2, the viability showed a slight dose-dependent decrease after 24 h incubation and a statistically significant reduction in cellular viability after 48 and 72 h of incubation.

DFX arrested the cell cycle at G1 phase in cervical cancer cell lines

To explore the mechanism of the anti-proliferative activity of DFX, the cell cycle was examined by flow cytometry. The results are shown in Figure 3a. The percentage of G1 phase cells increased from 47.83% to 68.19% after treatment with the indicated concentration of DFX (0–200 μM) in HeLa cells. A similar situation was observed in SiHa cells. To further verify the cell cycle results, we detected the effects of DFX on the protein levels of key cell cycle regulators such as cyclin D1, cyclin E, and PCNA. As seen in Figure 3b, incubation with DFX (0–200 μM) for 48 h gradually resulted in decreasing amounts of cyclin D1, cyclin E, and PCNA in both cell lines compared with control cells, thus confirming that DFX arrested the cell cycle.

DFX induced apoptosis in cervical cancer cell lines

Furthermore, we investigated the effects of DFX on apoptosis in HeLa and SiHa cells. After treatment with indicated concentrations of DFX (0–200 μM) for 48 h, the apoptotic cell ratio in HeLa and SiHa cells was determined by flow cytometry. Results showed that, compared with control cells, treatment with DFX increased the ratio of early apoptotic cells from 2.97% to 9.88%, and the ratio of late apoptotic cells from 1.27% to 16.21% in HeLa cells (Figure 4). A similar result was observed in SiHa cells. These data indicate that DFX inhibits the proliferation of cervical cancer cells by arresting the cell cycle in the G1 phase and inducing cell apoptosis.

DFX inhibits the invasion ability of cervical cancer cells by upregulating the expression of NDRG1 and downregulating the expression of c-myc

The effect of DFX on the invasion of cervical cancer cell lines was evaluated using Transwell chambers. As shown in Figure 5a, DFX significantly decreased invasion of HeLa and SiHa cells by approximately 5-fold compared with control cells.

NDRG1 is defined as a metastasis suppressor and can be downregulated in many types of cancer, and is thought to be an indication of tumor progression in a variety of cancers [13]. The c-myc gene is amplified and upregulated in many human tumors and plays an important role in their malignant regulation, proliferation, and metastasis [14]. The mRNA and protein levels of NDRG1 and c-myc were measured by RT-PCR and western blot after treatment with 0, 50, and 100 μM DFX for 48 h in HeLa and SiHa cells. Results showed that DFX significantly increased the mRNA and protein levels of NDRG1 in both cell lines, while the mRNA and protein levels of c-myc were decreased compared with control cells (Figure 5b and c). These results demonstrated that DFX inhibits the invasion of cervical cancer cells by regulating the expression of NDRG1 and c-myc.

DFX inhibits the activation of the MEK/ERK signaling pathway

It has been reported that the MEK/ERK signaling pathway plays an important role in cancer development and progression [15, 16]. We further investigated the effect of DFX on the activation of the MEK/ERK signaling pathway. As shown in Figure 6, HeLa and SiHa cells were incubated with DFX (50 μM) for 0–60 min, and the protein levels of p-Raf, p-MEK, and p-ERK were detected by western blotting. DFX suppressed the protein levels of p-Raf, p-MEK, and p-ERK in both cell lines after 30 min of treatment, and was most significant at 60 min compared with the control. These results suggested that DFX arrested cell cycle progression and inhibited proliferation and invasion of cervical cancer cells by inhibiting the activation of the MEK/ERK signaling pathway.

DFX inhibited tumor growth of human cervical cancer xenografts in nude mice

The anti-proliferative activity of DFX against cervical cancer was assessed in *vivo* using HeLa cervical cancer xenografts in BALB/c nude mice. After 14 days of injection of HeLa cells, no significant differences were observed in the xenograft tumor volumes and body weights. Engrafted mice (average tumor volume 150 mm^3) were randomly divided into three groups: control, DFX (100 mg/kg), and DFX (200 mg/kg) groups.

As shown in Figure 7a and b, 100 mg/kg DFX significantly inhibited tumor growth after 24 days of treatment, compared with the control group. DFX (200 mg/kg) significantly inhibited tumor growth after 14 days of treatment. One week after the end of the treatment (day 42), the tumor volumes decreased by 19.9% and 63.8% after DFX 100 and 200 mg/kg treatment, respectively.

At day 43, all tumors were dissected and measured (Figure 7c and d). The results showed that the weight of tumors in the 200 mg/kg DFX group was decreased by approximately 40% compared with that in the control group. Furthermore, there were no serious effects on mice body weight (Figure 7e).

DFX down-regulates serum ferritin levels in nude mice bearing HeLa cell xenografts and inhibits FTH protein levels in xenografts

We further detected the serum indices in nude mice bearing HeLa xenografts. As shown in Table 1, DFX (200 mg/kg) significantly decreased serum ferritin levels from 20.29 ± 1.42 to 10.24 ± 1.74 ng/mL, compared with the control group. Other hematological parameters did not show significant alterations. Furthermore, DFX significantly reduced the expression of FTH compared with the control group ($p < 0.05$) (Figure 8).

Discussion

Iron is required for cell proliferation [17]. Cancer cells have a higher requirement for iron because of their rapid proliferation [4, 17]. Iron chelators have been used for the treatment of iron-overload disease [18]. DFO and DFX are two licensed iron chelators commonly used for iron-overload disease [19, 20]. DFO has been reported to inhibit the growth of cervical cancer cells [11], but it failed to prevent the growth of cervical carcinoma xenografts in mice [12]. DFO cannot be administered orally and has a short serum

half-life, thus limiting its clinical application [20, 21]. This may be the reason why DFO failed to prevent the growth of cervical carcinoma xenografts in mice. DFX is an oral iron chelator that has been successfully used in clinical trials in iron-overload patients [22]. It can be administered orally, with steady-state concentrations in serum achieved within three days [23]. Previous reports have shown that DFX has anti-proliferative activity against numerous types of solid tumors and cell culture, such as murine leukemia, lung tumor, esophageal cancer, pancreatic cancer and hepatocellular carcinoma [24–27, 6, 7]. However, no study has investigated the effects of DFX on cervical cancer. In the present study, we demonstrated the inhibitory effect of DFX against cervical cancer cells and cervical carcinoma xenografts in mice for the first time.

Increased levels of serum ferritin have been reported in a wide range of malignancies [28, 29]. The levels of serum ferritin in patients with cervical cancer are elevated [30]. Tissue ferritin in cytosol extracts from mammary carcinomas showed up to a 10-fold increase in breast cancer [31]. The level of ferritin in tumor tissues of patients with cervical cancer has not been reported. In the present study, we investigated the levels of ferritin in the serum and tumor tissues of patients with cervical cancer. Results showed that serum ferritin concentration in cervical cancer group patients was higher than that in cervical intraepithelial neoplasia and normal cervical epithelial group patients (Figure S1 a). We also observed increased FTH protein expression in the tissue sections of patients with cervical cancer (Figure S1 b). The increase in serum ferritin levels in patients with cervical cancer is in accordance with a previous report [28–30]. These results confirmed that the occurrence and development of cervical cancer is related to changes in iron metabolism.

We then tested the effect of DFX on iron metabolism regulators in cervical cancer cells. Results showed that TfR1 protein levels were increased, while FTH protein levels were decreased by DFX treatment in the HeLa and SiHa cervical cancer cell lines in a dose-dependent manner (Fig. 1). This result demonstrates the iron chelation function of DFX in HeLa and SiHa cells. We also demonstrated the anti-proliferative activity of DFX in HeLa and SiHa cells in a dose- and time-dependent manner (Fig. 2).

Iron is crucial for cell growth [17]. Iron depletion leads to cell cycle G1/S arrest and apoptosis [32]. Previous reports have shown that DFX arrested the cell cycle at the G0/G1 and S phases in acute myeloid leukemia cell lines and pancreatic cancer cell lines [6, 7]. DFX also causes apoptosis in proximal tubular cells, murine leukemia cell lines, and pancreatic cancer cell lines [5, 7, 33]. To investigate the mechanisms of the anti-proliferative activity of DFX, we examined the effects of DFX on the cell cycle and apoptosis in HeLa and SiHa cells. We observed that DFX arrested the cell cycle in the G0/G1 phase (Fig. 3a) and downregulated critical molecules for cell cycle progression, such as cyclin D1, cyclin E, and PCNA, in a dose-dependent manner (Fig. 3b). Furthermore, we also determined that DFX induced apoptosis in HeLa and SiHa cells (Fig. 4). These results suggest that the anti-proliferative effect of DFX against cervical cancer cells is due to cell cycle inhibition by affecting the expression of critical molecules and apoptosis induction.

Additionally, migration and invasion are of great significance for effectively controlling tumor development and reducing mortality in many cancers [34]. NDRG1 and c-myc function as two critical regulators of cancer cell invasion and metastasis [35–37]. Iron chelators DFO and Dp44mT attenuate TGF-β-induced migration and invasion in HT29 and DU145 cells [38]. The present study showed that DFX significantly decreased the invasion of HeLa and SiHa cells, when compared with untreated control cells (Fig. 5a). Meanwhile, DFX increased the mRNA and protein levels of NDRG1, and decreased the mRNA and protein levels of c-myc (Fig. 5b and c).

The MEK/ERK signaling pathway regulates cell proliferation, cell cycle, apoptosis, migration, invasion, and many other biological processes [39–41]. Activation of the MEK/ERK signaling pathway is associated with tumor occurrence, progression, and metastasis [42, 43]. Thus, we examined the effects of DFX on the ativation of the MEK/ERK signaling pathway in HeLa and SiHa cells. We found that DFX reduced the levels of p-ERK in HeLa and SiHa cells in a dose-dependent manner compared with control cells (Fig. 6). It also inhibited the activation of Raf and MEK, the upstream protein kinases of ERK. The findings of the current study indicate that DFX inhibited proliferation and invasion of cervical cancer cell lines by inhibiting the MEK/ERK signaling pathway.

Previous studies have demonstrated that DFX suppresses tumor xenografts of murine leukemia cells, esophageal adenocarcinoma cell lines, and human pancreatic cancer cell lines [25, 7, 41]. We finally assessed the ability of DFX to inhibit tumor growth in *vivo* using a HeLa cell xenograft model in mice. Results showed that 200 mg/kg DFX significantly inhibited HeLa cell xenografts (Fig. 7a-d). There was no weight loss in DFX-treated mice compared with controls (Fig. 7e). Meanwhile, the level of serum ferritin (Table 1) and the expression of FTH in tumor tissue (Fig. 8) decreased significantly in the DFX treatment group. All mice showed no signs of ill health and apparent adverse effects during the treatment period. No notable toxicity was found in the tissues of the liver, heart, lung, and intestine in mice treated with DFX (200 mg/kg) (Figure S2). Liver and renal function tests were normal, and all other hematological parameters were not significantly altered (Table 1).

Conclusions

Our study is the first to demonstrate the inhibitory activity of DFX against cervical cancer in *vitro* and in *vivo*. Our experimental results indicated that DFX inhibits cervical cancer cell proliferation by arresting the cell cycle and inducing cell apoptosis. Furthermore, DFX suppresses invasion of cervical cancer cells. These effects appeared to be related to the inhibition of the MEK/ERK signaling pathway. Finally, DFX suppressed xenograft tumor growth of cervical cancer in *vivo* without detectable negative side effects. However, further studies are needed to elucidate the exact mechanisms of the inhibitory activity of DFX against cervical cancer in *vitro* and in *vivo*. The results from the current study suggest that the DFX treatment strategy can be considered a novel, effective, and safe cervical cancer therapy in the future.

Abbreviations

DFX, deferasirox; PCNA, proliferating cell nuclear antigen; NDRG1, N-myc downstream regulated gene 1; FTH, ferritin heavy chain; DFO, deferoxamine; TfR1, transferrin receptor 1; ATCC, American Type Culture Collection; CCK-8, Cell counting kit-8; PI, propidium iodide; WBC, white blood cells; RBC, red blood cells; IHC, immunohistochemistry; FPN1, ferroportin 1.

Declarations

Acknowledgments

Not applicable.

Funding

This work was supported by Hebei Scientific Research Foundation for Returned Scholars (C201814), key projects of Hebei Normal University (L2018Z07), the National Natural Science Foundation of China (31701006)the One Hundred Person Project of Hebei Province (E2016100019, E2018050011).

Availability of data and materials

The datasets used and/or analyzed during the current study are available from the corresponding author on reasonable request.

Authors' contributions

YF and KT designed the study and participated in manuscript preparation. NZ and CY performed the experiments and prepared the manuscript. YK, JH, YZ, SC and XX participated in the experiments performance and data analysis. PC and XD approved the manuscript editing. All authors read and approved the final manuscript.

Competing interests

The authors declare that they have no competing interest.

Consent for publication

Not applicable

Ethics approval and consent to participate

The animal experimental protocol was established according to the ARRIVE guidelines and was approved by the Laboratory Animal Ethical and Welfare CommitteeAEWCof Hebei Normal University. The human study was designed and performed in accordance with the Declaration of Helsinki and approved by the Ethics Committee of Xingtai People's Hospital.

References

1. Aydinok Y, Kattamis A, Cappellini MD, El-Beshlawy A, Origa R, Elalfy M, et al. Effects of deferasirox-deferoxamine on myocardial and liver iron in patients with severe transfusional iron overload. Blood. 2015;125(25):3868–77.
2. Bentur Y, McGuigan M, Koren G. Deferoxamine (desferrioxamine). New toxicities for an old drug. Drug Saf. 1991;6(1):37–46.
3. Bollig C, Schell LK, Rücker G, Allert R, Motschall E, Niemeyer CM, et al. Deferasirox for managing iron overload in people with thalassaemia. Cochrane Database Syst Rev. 2017;8(8):CD007476.
4. Brissot P, Pietrangelo A, Adams C, de Graaff B, McLaren CE. Loréal O. Haemochromatosis. Nat Rev Dis Primers. 2018;4:18016.
5. Chang YC, Lo WJ, Huang YT, Lin CL, Feng CC, Lin HT, et al. Deferasirox has strong anti-leukemia activity but may antagonize theanti-leukemia effect of doxorubicin. Leuk Lymphoma. 2017;58(9):1–12.
6. Chen JB, Zhang M, Zhang XL, Cui Y, Liu PH, Hu J, et al. Glucocorticoid-Inducible Kinase 2 Promotes Bladder Cancer Cell Proliferation, Migration and Invasion by Enhancing β-catenin/c-Myc Signaling Pathway. J Cancer. 2018;9(24):4774–82.
7. Chen Z, Zhang D, Yue F, Zheng M, Kovacevic Z, Richardson DR. The Iron Chelators Dp44mT and DFO Inhibit TGF-β-induced Epithelial-Mesenchymal Transition via Up-Regulation of N-Myc Downstream-regulated Gene 1 (NDRG1). J Biol Chem. 2012;287(21):17016–28.
8. Ciccarelli C, Di Rocco A, Grabina GL, Mauro A, Festuccia C, Del Fattore A, et al. Disruption of MEK/ERK/c-Myc signaling radiosensitizes prostate cancer cells in *vitro* and in *vivo*. J Cancer Res Clin Oncol. 2018;144(9):1685–99.
9. Degirmenci U, Wang M, Hu J. Targeting Aberrant RAS/RAF/MEK/ERK Signaling for Cancer Therapy. Cells. 2020;9(1):pii: E198.
10. Ford SJ, Obeidy P, Lovejoy DB, Bedford M, Nichols L, Chadwick C, et al. Deferasirox (ICL670A) effectively inhibits esophageal cancer growth in *vitro* and in *vivo*. Br J Pharmacol. 2013;168(6):1316–28.
11. Guo ZL, Richardson DR, Kalinowski DS, Kovacevic Z, Tan-Un KC, Chan GC. The novel thiosemicarbazone, di-2-pyridylketone 4-cyclohexyl-4-methyl-3-thiosemicarbazone (DpC), inhibits neuroblastoma growth in vitro and in vivo via multiple mechanisms. J Hematol Oncol. 2016;9(1):98.
12. Hamilton JL, Imran Ul-Haq M, Abbina S, Kalathottukaren MT, Lai BF, Hatef A, et al. In vivo efficacy, toxicity and biodistribution of ultra-long circulating desferrioxamine based polymeric iron chelator. Biomaterials. 2016;102:58–71.
13. Harima H, Kaino S, Takami T, Shinoda S, Matsumoto T, Fujisawa K, et al. Deferasirox, a novel oral iron chelator, shows antiproliferative activity against pancreatic cancer in vitro and in vivo. BMC Cancer. 2016;16(1):702.

14. Ito H, Takaqi Y, Ando Y, Kubo A, Hashimoto S, Tsutsui F, Kurihara S. Serum ferritin levels in patients with cervical cancer. Obstet Gynecol. 1980;55(3):358–62.
15. Javed S, Sharma BK, Sood S, Sharma S, Bagga R, Bhattacharyya S, et al. Significance of CD133 positive cells in four novel HPV-16 positive cervical cancer derived cell lines and biopsies of invasive cervical cancer. BMC Cancer. 2018;18(1):357.
16. Jeon SR, Lee JW, Jang PS, Chung NG, Cho B, Jeong DC. Anti-leukemic properties of deferasirox via apoptosis in murine leukemia cell lines. Blood Res. 2015;50(1):33–9.
17. Jung M, Mertens C, Tomat E, Brüne B. Iron as a Central Player and Promising Target in Cancer Progression. Int J Mol Sci. 2019;20(2):273.
18. Ko BS, Chang MC, Chiou TJ, Chang TK, Chen YC, Lin SF, et al. Long-term safety and efficacy of deferasirox in patients with myelodysplastic syndrome, aplastic anemia and other rare anemia in Taiwan. Hematology. 2019;24(1):247–54.
19. Lee DH, Janq PS, Chung NG, Cho B, Jeong DC, Kim HK. Deferasirox shows in *vitro* and in *vivo* antileukemic effects on murine leukemic cell lines regardless of iron status. Exp Hematol. 2013;41(6):539–46.
20. Lee S, Song A, Eo W. Serum Ferritin as a Prognostic Biomarker for Survival in Relapsed or Refractory Metastatic Colorectal. J Cancer. 2016;7(8):957–64.
21. Lui GY, Obeidy P, Ford SJ, Tselepis C, Sharp DM, Jansson PJ, et al. The iron chelator, deferasirox, as a novel strategy for cancer treatment: oral activity against human lung tumor xenografts and molecular mechanism of action. Mol Pharmacol. 2013;83(1):179–90.
22. Luo P, Zhang C, Liao F, Chen L, Liu Z, Long L, et al. Transcriptional positive cofactor 4 promotes breast cancer proliferation and metastasis through c-Myc mediated Warburg effect. Cell Commun Signal. 2019;17(1):36.
23. Martin-Sanchea D, Galleqos-Villalobos A, Fontecha-Barriuso M, Carrasco S, Sanchez-Niño MD, Lopez-Hernandez FJ, et al. Deferasirox-induced iron depletion promotes BclxL down-regulation and death of proximal tubular cells. Sci Rep. 2017;7:41510.
24. Mi L, Zhu F, Yang X, Lu J, Zheng Y, Zhao Q, et al. The metastatic suppressor NDRG1 inhibits EMT, migration and invasion through interaction and promotion of caveolin-1 ubiquitylation in human colorectal cancer cells. Oncogene. 2017;36(30):4323–35.
25. Mrklas KJ, MacDonald S, Shea-Budgell MA, Bedingfield N, Ganshorn H, Glaze S, et al. Barriers, supports, and effective interventions for uptake of human papillomavirus- and other vaccines within global and Canadian indigenous peoples: a systematic review protocol. Syst Rev. 2018;7(1):40.
26. Nishitani S, Noma K, Ohara T, Tomono Y, Watanabe S, Tazawa H, et al. Iron depletion-induced downregulation of N-cadherin expression inhibits invasive malignant phenotypes in human esophageal cancer. Int J Oncol. 2016;49(4):1351–9.
27. Wangpu X, Lu JY, Xi RX, Yue F, Sahni S, Park KC, et al. Targeting the Metastasis Suppressor, N-Myc Downstream Regulated Gene-1, with Novel Di-2-Pyridylketone Thiosemicarbazones: Suppression of

Tumor Cell Migration and Cell-Collagen Adhesion by Inhibiting Focal Adhesion Kinase/Paxillin Signaling. Mol Pharmacol. 2016;89(5):521–40.

28. Quintana Pacheco DA, Sookthai D, Graf ME, Schubel R, Johnson T, Katzke VA, et al. Iron status in relation to cancer risk and mortality: Findings from a population-based prospective study. Int J Cancer. 2018;143(3):561–9.
29. Saeki I, Yamamoto N, Yamasaki T, Takami T, Maeda M, Fujisawa K, et al. Effects of an oral iron chelator, deferasirox, on advanced hepatocellular carcinoma. World J Gastroenterol. 2016;22(40):8967–77.
30. Sharma A, Mendonca J, Ying J, Kim HS, Verdone JE, Zarif Jelani C, et al. The prostate metastasis suppressor gene NDRG1 differentially regulates cell motility and invasion. Mol Oncol. 2017;11(6):655–69.
31. Sidarovich V, Adami V, Gatto P, Greco V, Tebaldi T, Tonini GP, Quattrone A. Translational down-regulation of HSP 90 expression by iron chelators in neuroblastoma cells. Mol Pharmacol. 2015;87(3):513–24.
32. Simonart T, Boelaert Johan R, Mosselmans R, Andrei G, Noel JC, et al. Antiproliferative and apoptotic effects of iron chelators on human cervical carcinoma cells. Gynecol Oncol. 2002;85(1):95–102.
33. Simonart T, Boelaert JR, Andrei G, Clercg ED, Snoeck R. Iron withdrawal strategies fail to prevent the growth of SiHa-induced tumors in mice. Gynecol Oncol. 2003;90(1):91–5.
34. Small W Jr, Bacon MA, Bajaj A, Chuang LT, Fisher BJ, et al. Cervical cancer: A global health crisis. Cancer. 2017;123(13):2404–12.
35. Tian X, Geng J, Zheng Q, Wang L, Huang P, Tong J, Zheng S. Single high dose irradiation induces cell cycle arrest and apoptosis in human hepatocellular carcinoma cells through the Ras/Raf/MEK/ERK pathways. Int J Radiat Biol. 2020;96(6):740–7.
36. Torti SV, Manz DH, Paul BT, Blanchette-Farra N, Torti FM. Iron and Cancer. Annu Rev Nutr. 2018;38:97–125.
37. Vitrano A, Ruffo GB, Pepe A, D'Ascola DG, Caruso V, Filosa A, et al. Long-termsequential deferiprone and deferasirox therapy in transfusion-dependent thalassaemia patients: a prospective clinical trial. Br J Haematol. 2019;186(6):e209–11.
38. Wang F, Lv H, Zhao B, Zhou L, Wang S, Luo J, et al. Iron and leukemia: new insights for future treatments. J Exp Clin Cancer Res. 2019;38(1):406.
39. Weinstein RE, Bond BH, Silberberq BK. Tissue ferritin concentration in carcinoma of the breast. Cancer. 1982;50(11):2406–9.
40. Yamaguchi H, Wyckoff J, Condeelis J. Cell migration in tumors. Curr Opin Cell Biol. 2005;17(5):559–64.
41. Yu Y, Kovacevic Z, Richardson DR. Tuning cell cycle regulation with an iron key. Cell Cycle. 2007;6(61):1982–94.

42. Zeng B, Shi W, Tan G. MiR-199a/b-3p inhibits gastric cancer cell proliferation via down-regulating PAK4/MEK/ERK signaling pathway. BMC Cancer. 2018;18(1):34.
43. Zhang R, Shi H, Ren F, Feng W, Cao Y, Li G, et al. MicroRNA-338-3p suppresses ovarian cancer cells growth and metastasis: implication of Wnt/catenin beta and MEK/ERK signaling pathways. J Exp Clin Cancer Res. 2019;38(1):494.

Figures

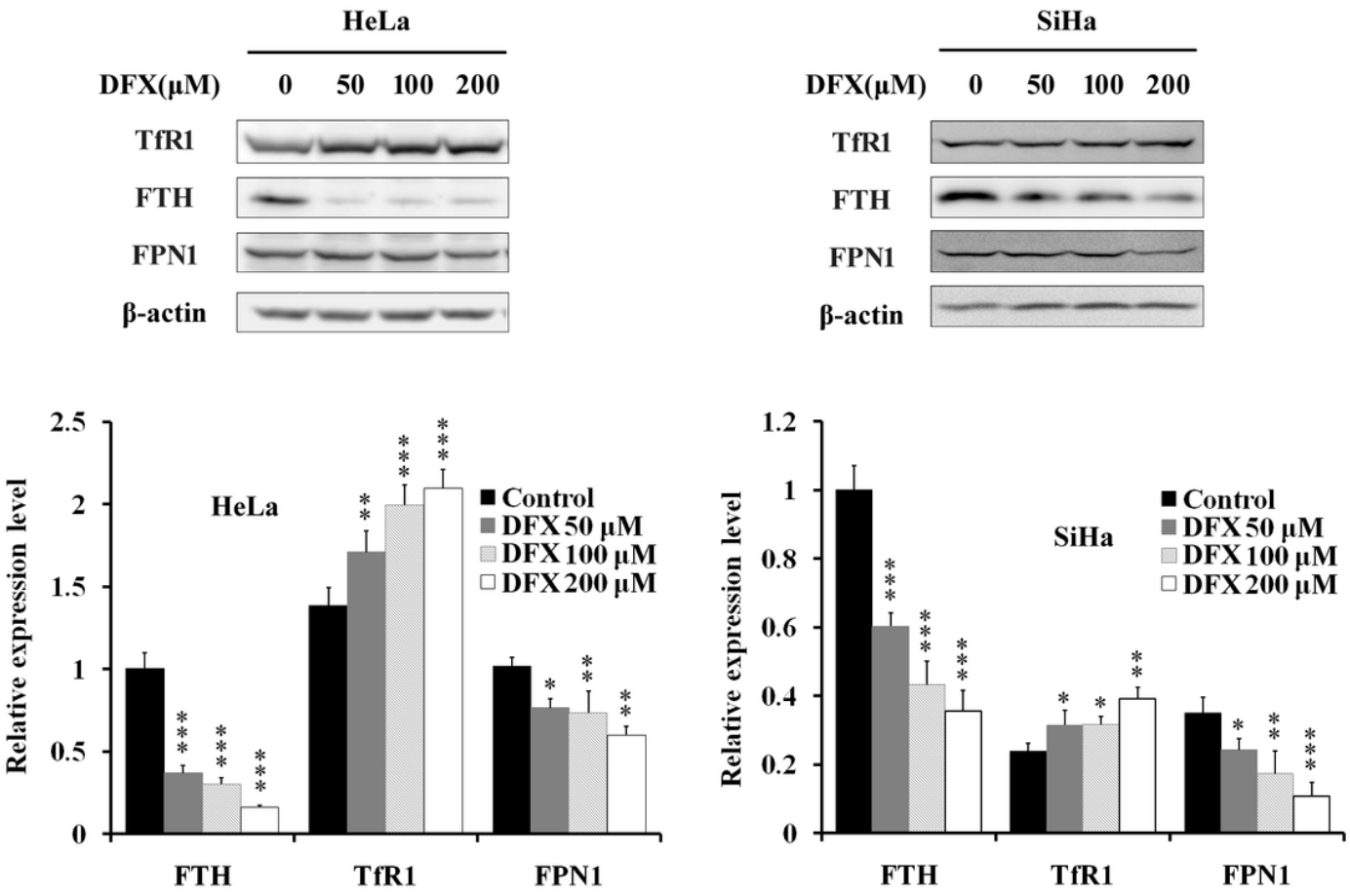

Figure 1

Effects of DFX on the expression of TfR1, FTH, and FPN1. HeLa and SiHa cells were incubated with DFX (0–200 μM) for 48 h. The protein levels of TfR1, FTH, and FPN1 were detected by western blot. β-actin was used as a loading control. *p < 0.05, **p < 0.01, ***p < 0.001, * vs. Control. The experiments were repeated three times, and similar results were obtained. The figure shows representative results.

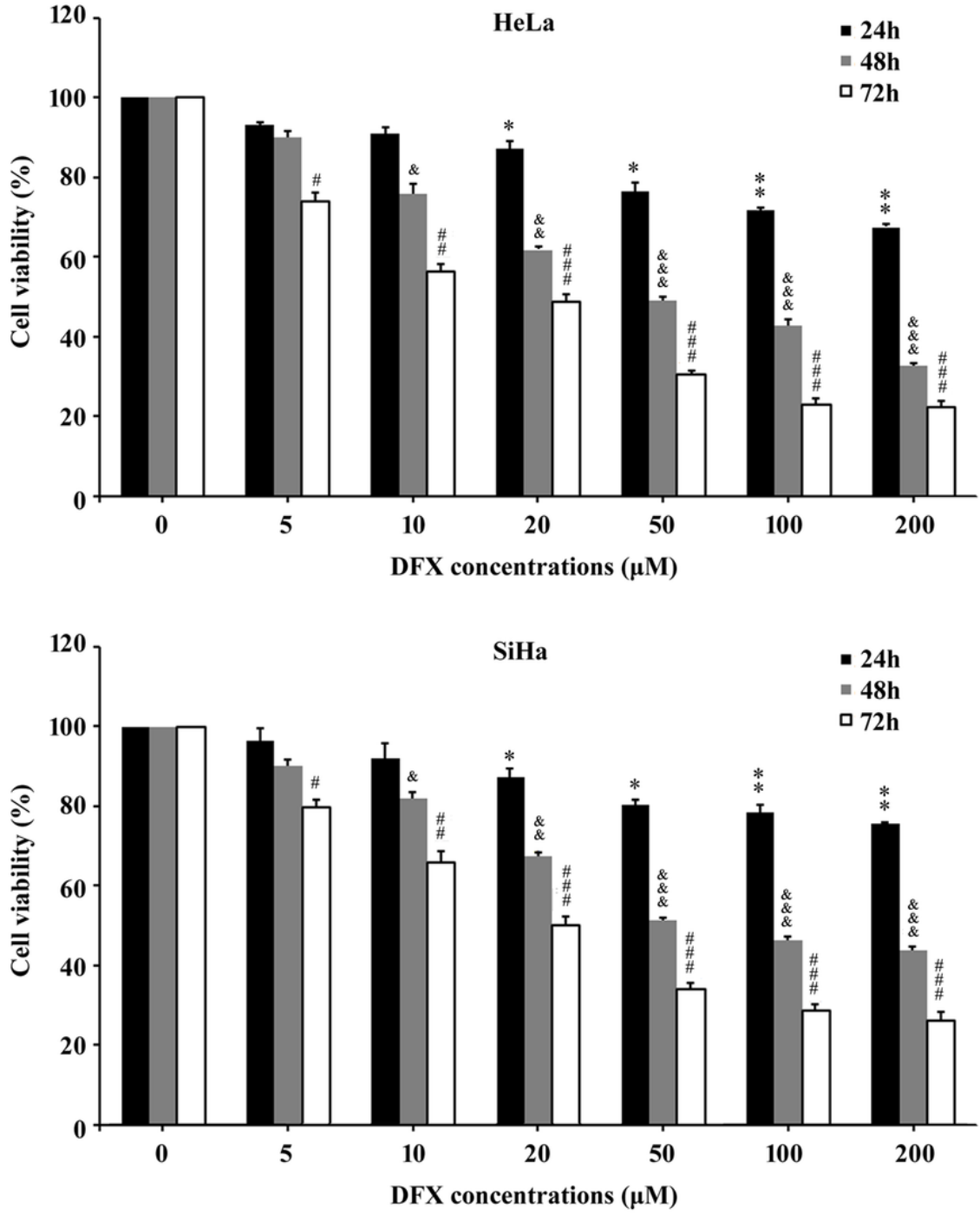

Figure 2

Effects of DFX on cervical cancer cell viability. HeLa and SiHa cells were treated with DFX (0–200 μM) for indicated times. Cell viability was assessed using the CCK-8 assay. The data are presented as the mean ± SEM (three experiments). *p < 0.05, **p < 0.01, * vs. 24 h group without DFX treatment; &p < 0.05, &&p < 0.01, &&&p < 0.001, & vs. 48 h group without DFX treatment; #p < 0.05, ##p < 0.01, ###p < 0.001, # vs. 72 h group without DFX treatment.

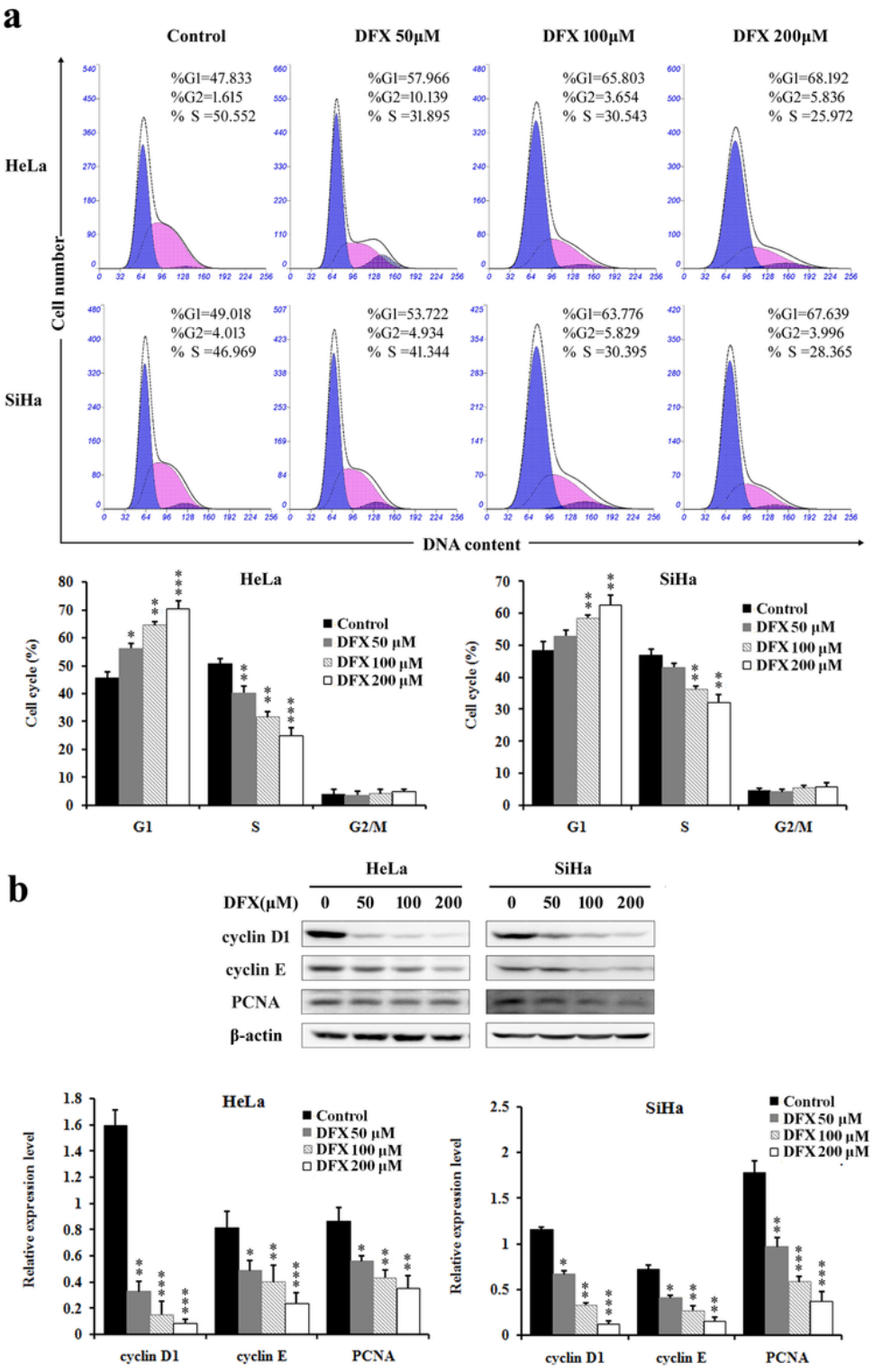

Figure 3

Effects of DFX on cervical cancer cell cycle. HeLa and SiHa cells were incubated with the indicated conditions of DFX (0–200 μM) for 48 h. (a) The cell cycle was analyzed by flow cytometry. (b) The expression of key regulators of cell cycle cyclin D1, cyclin E, and PCNA were detected by western blot. β-actin was used as a loading control. *p < 0.05, **p < 0.01, ***p < 0.001, * vs. Control. The experiments were repeated three times, and similar results were obtained. The figure shows representative results.

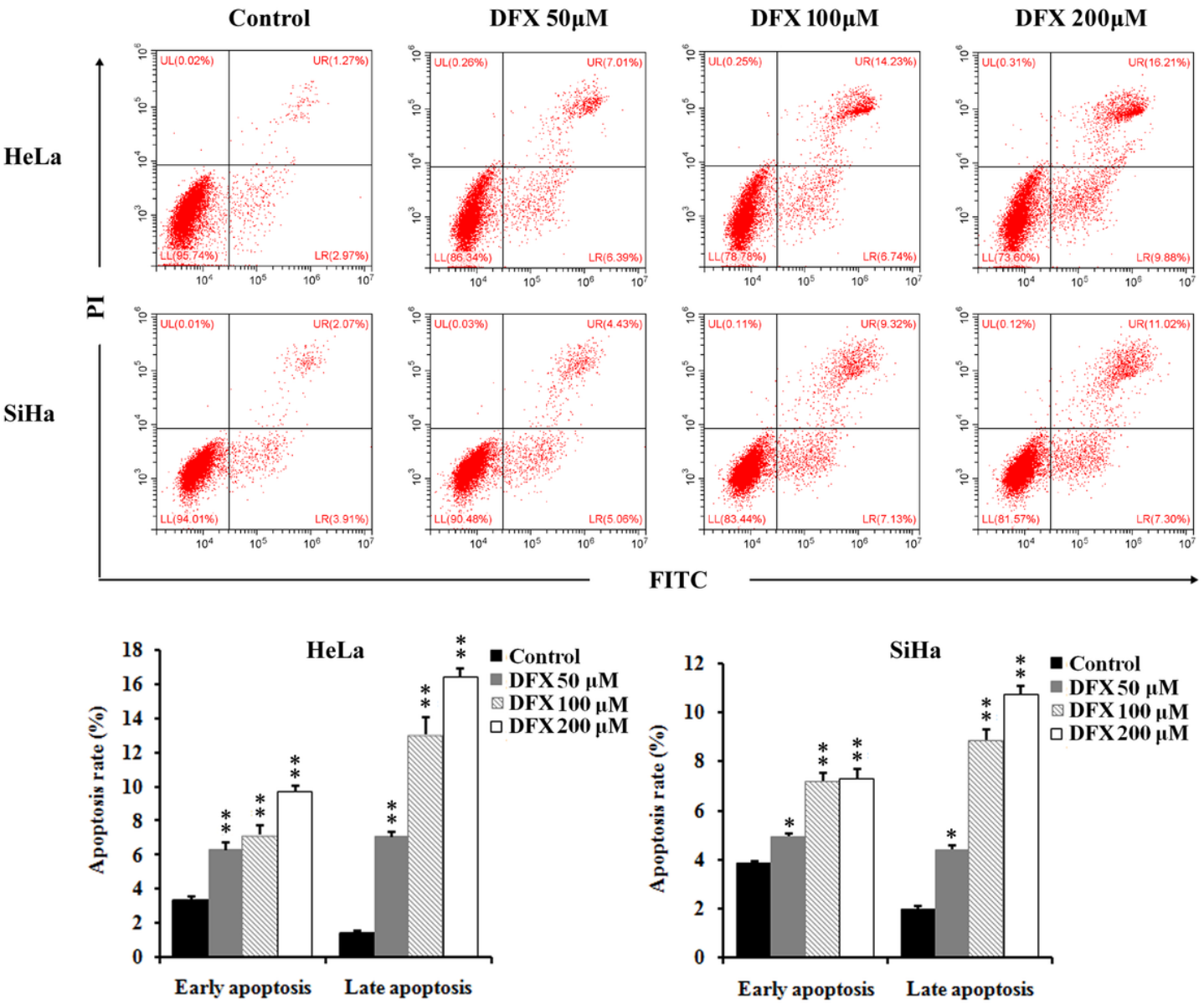

Figure 4

Effects of DFX on apoptosis of cervical cancer cells. HeLa and SiHa cells were incubated with the indicated conditions of DFX (0–200 μM) for 48 h. The early and late cell apoptosis ratio was analyzed by flow cytometry. *p < 0.05, **p < 0.01, * vs. Control. The experiments were repeated three times, and similar results were obtained. The figure shows representative results.

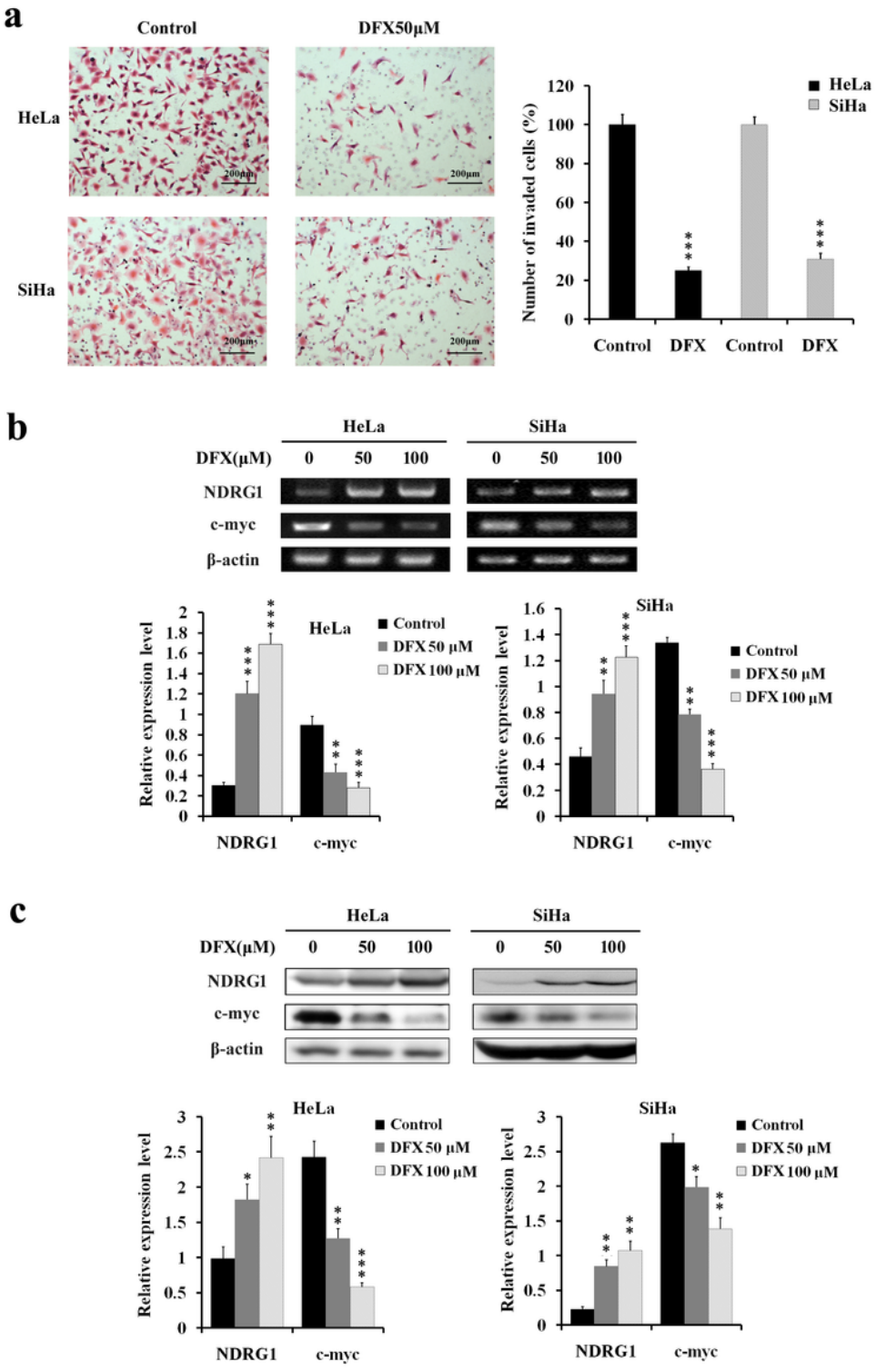

Figure 5

Effects of DFX on the invasion ability of cervical cancer cells. (a) The invasion ability of HeLa and SiHa cells was measured by the Transwell assay, as described in Materials and Methods. HeLa and SiHa cells were incubated with the indicated conditions of DFX (0–100 μM) for 24 h. The mRNA and protein levels of NDRG1 and c-myc were determined by RT-PCR (b) and western blot (c). β-actin was used as an internal

control. *p < 0.05, **p < 0.01, ***p < 0.001, * vs. Control. The experiments were repeated three times, and similar results were obtained. The figure shows representative results.

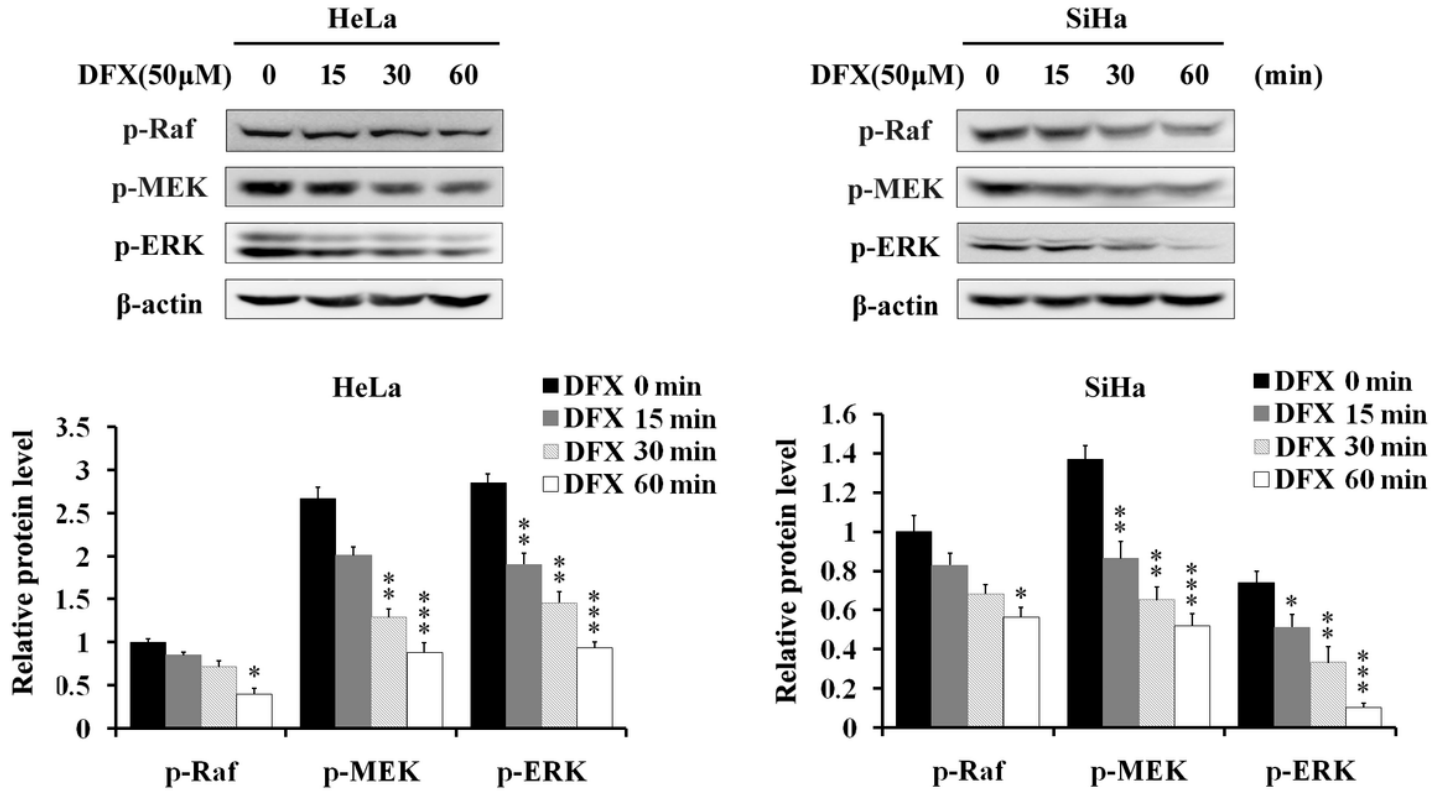

Figure 6

Effects of DFX on the activation of the MEK/ERK signaling pathway. HeLa and SiHa cells were exposed to 50 μM DFX for the indicated times (0–60 min). The protein levels of p-Raf, p-MEK, and p-ERK were detected by western blot. β-actin was used as a loading control. *p < 0.05, **p < 0.01, ***p < 0.001, * vs. DFX-untreated cells. The experiments were repeated three times, and similar results were obtained. The figure shows representative results.

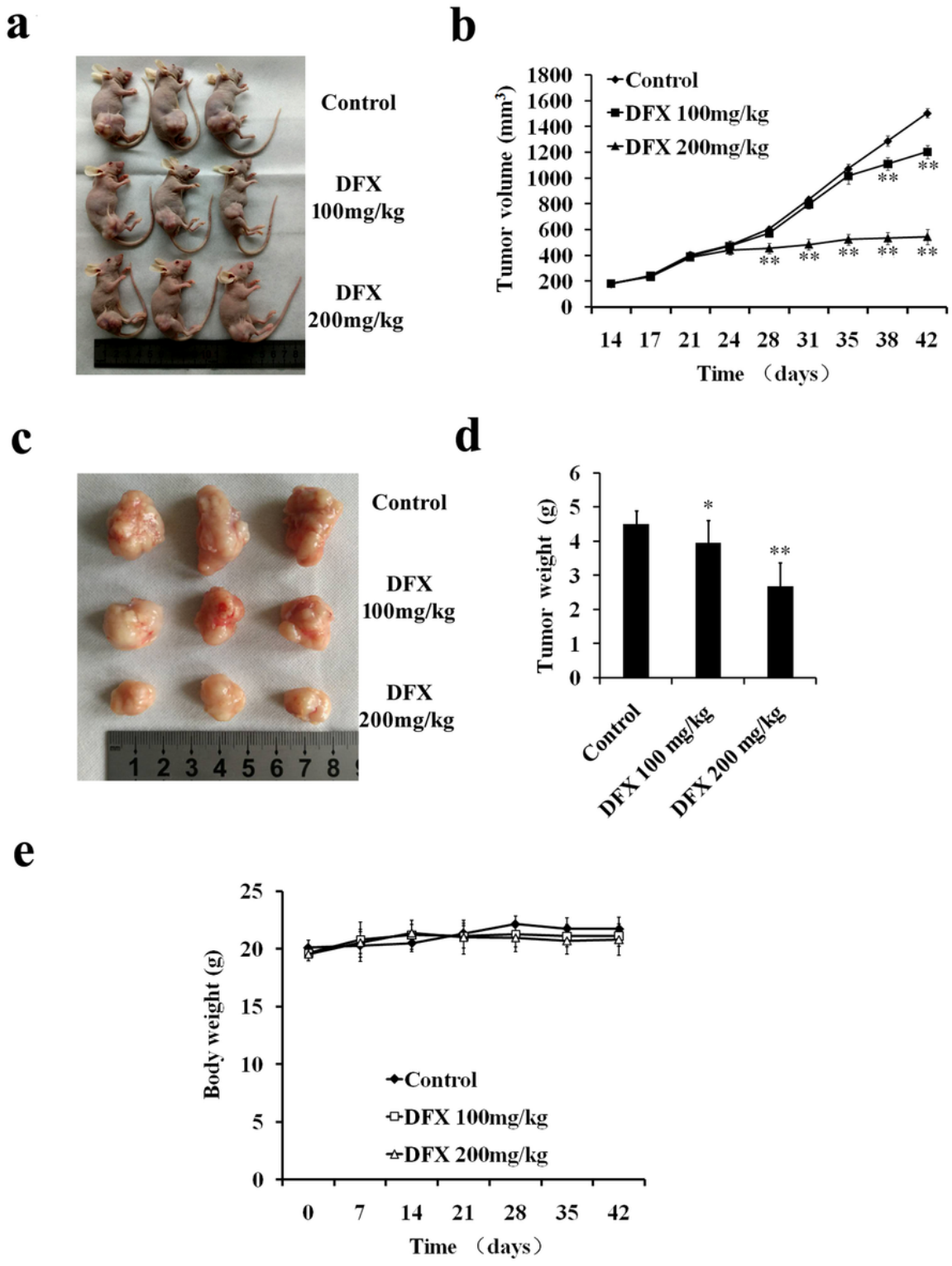

Figure 7

Effect of DFX on murine xenograft growth. Tumor xenografts of HeLa cells were generated as described in Materials and Methods. DFX (100 mg/kg and 200 mg/kg) was orally administered every other day for 3 weeks. (a) Representative images of tumor-bearing mice. (b) Tumor sizes of the three groups. (c) Representative images of excised tumors from mice. (d) Evaluation of weight of the excised mice tumors

from each treatment group. (e) The average body weight of mice in each treatment group during the course of treatment. *p < 0.05, **p < 0.01, * vs. DFX-untreated group.

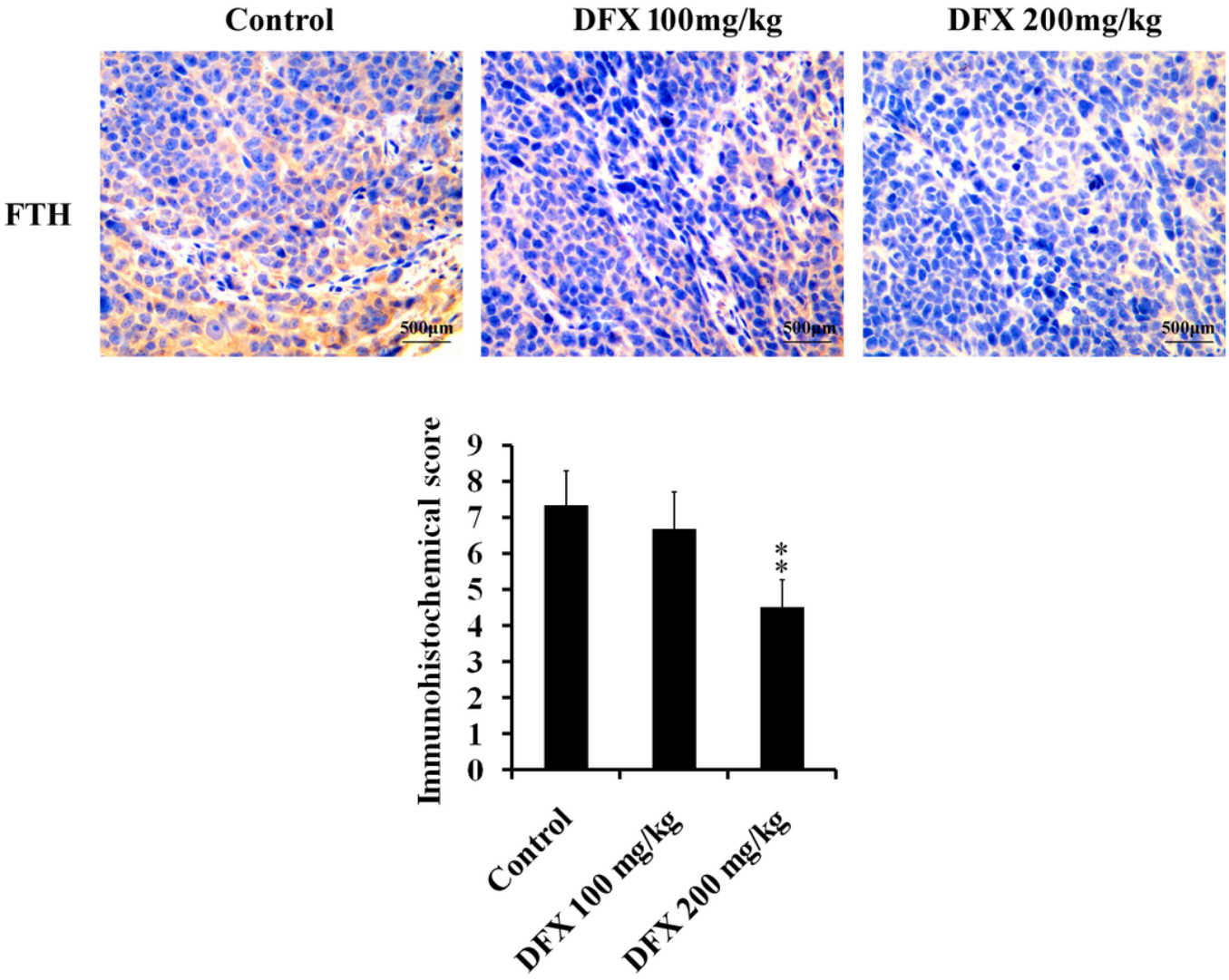

Figure 8

Effect of DFX on serum ferritin levels in nude mice bearing HeLa cell xenografts and FTH protein levels in xenografts. Tumor xenografts of HeLa cells were generated as described in Materials and Methods. DFX (100 mg/kg and 200 mg/kg) was orally administered every other day for 3 weeks. FTH protein levels in the removed tumors were determined by immunohistochemical analyses. **p < 0.01, * vs. DFX-untreated group.

Supplementary Files

This is a list of supplementary files associated with this preprint. Click to download.

- Supportingdocuments.docx

- WesternBlotPDFforReview.pdf
- NC3RsARRIVEGuidelinesChecklistfillable.pdf